J|A|C|S
ARTICLES
Published on Web 01/21/2003

Density Functional and Reduction Potential Calculations of Fe_4S_4 Clusters

Rhonda A. Torres, Timothy Lovell, Louis Noodleman,* and David A. Case*

Contribution from the Department of Molecular Biology TPC-15, The Scripps Research Institute, La Jolla, California 92037

Received August 22, 2002; Revised Manuscript Received November 21, 2002; E-mail: lou@scripps.edu; case@scripps.edu

Abstract: Density functional theory geometry optimizations and reduction potential calculations are reported for all five known oxidation states of $[Fe_4S_4(SCH_3)_4]^{n-}$ ($n = 0, 1, 2, 3, 4$) clusters that form the active sites of iron−sulfur proteins. The geometry-optimized structures tend to be slightly expanded relative to experiment, with the best comparison found in the $[Fe_4S_4(SCH_3)_4]^{2-}$ model cluster, having bond lengths 0.03 Å longer on average than experimentally observed. Environmental effects are modeled with a continuum dielectric, allowing the solvent contribution to the reduction potential to be calculated. The calculated protein plus solvent effects on the reduction potentials of seven proteins (including high potential iron proteins, ferredoxins, the iron protein of nitrogenase, and the "X", "A", and "B" centers of photosystem I) are also examined. A good correlation between predicted and measured absolute reduction potentials for each oxidation state of the cluster is found, both for relative potentials within a given oxidation state and for the absolute potentials for all known couples. These calculations suggest that the number of amide dipole and hydrogen bonding interactions with the Fe_4S_4 clusters play a key role in modulating the accessible redox couple. For the $[Fe_4S_4]^0$ (all-ferrous) system, the experimentally observed $S = 4$ state is calculated to lie lowest in energy, and the predicted geometry and electronic properties for this state correlate well with the EXAFS and Mössbauer data. Cluster geometries are also predicted for the $[Fe_4S_4]^{4+}$ (all-ferric) system, and the calculated reduction potential for the $[Fe_4S_4(SCH_3)_4]^{1-/0}$ redox couple is in good agreement with that estimated for experimental model clusters containing alkylthiolate ligands.

1. Introduction

The presence of iron−sulfur clusters in biological systems was only recognized approximately forty years ago;[1] however, the biological importance of these molecules has since been well established. Iron−sulfur clusters are ubiquitous in nature and play critical roles in electron transfer[2,3] and catalysis.[4] In some instances, these functions are combined, as in the case of oxidoreductase proteins, where substrate binding and catalytic transformations are associated with electron (and proton) transfer events.[5−8] The prevalence of these clusters is likely due to their modular nature, which allows them to accomplish this wide variety of functions. The physical properties of iron−sulfur clusters have been studied using a wide variety of spectroscopic, structural, and theoretical techniques in an effort to understand the physical properties and electronic structures of these clusters. Synthetic analogues representing iron−sulfur clusters in proteins have been shown to display similar structural features and reduction potentials[9] to their protein counterparts, although the protein reduction potentials are generally more positive.[10−14] The shift toward more positive potentials relative to the model systems is believed to be largely due to differences in the protein environment compared to the solvent environment rather than to structural changes in the clusters themselves. These differences aside, model systems of iron−sulfur clusters provide a basis for understanding the more complex redox associated properties of these cofactors in proteins. In particular, the four-iron "cubane" clusters, with an Fe_4S_4 core, are of interest, since they can be prepared in five oxidation states, ranging from (formally) all ferrous to all ferric. This allows us to test our calculations over a wide range of reduction potentials.

Quantum mechanical calculations are now a widely used method in the interpretation and prediction of both structural and electronic properties of transition metal complexes, particularly those containing two or more iron sites.[15−17] Special

(1) Beinert, H. *FASEB J.* **1990**, *4*, 2483−2491.
(2) Mitchell, P. *J. Biochem.* 1985, *97*, 1−18.
(3) Han, A. L.; Yagi, T.; Hatefi, Y. *Arch. Biochem. Biophys.* **1989**, *275*, 166−173.
(4) Beinert, H.; Kennedy, M. C.; Stout, C. D. *Chem. Rev.* **1996**, *96*, 2335−2373.
(5) Howard, J. B.; Rees, D. C. *Chem. Rev.* **1996**, *96*, 2965−2982.
(6) Lindahl, P. A.; Ragsdale, S. W.; Munck, E. *J. Biol. Chem.* 1990, *265*, 3880−3888.
(7) Qiu, D.; Kumar, M.; Ragsdale, S. W.; Spiro, T. G. *Science* **1994**, *264*, 817−819.
(8) Lindahl, P. A.; Kovacs, J. A. *J. Cluster Sci.* **1990**, *1*, 29−73.
(9) Holm, R. H.; Ibers, J. A. In *Iron Sulfur Proteins;* Lovenberg, W., Ed.; Academic Press: New York, 1977; Vol. 3, pp 205−281.
(10) Battistuzzi, G.; D'Onofrio, M.; Borsari, M.; Sola, M.; Macedo, A. L.; Moura, J. J. G.; Rodrigues, P. *JBIC, J. Biol. Inorg. Chem.* **2000**, *5*, 748−760.
(11) Mouesca, J.-M.; Chen, J. L.; Noodleman, L.; Bashford, D.; Case, D. A. *J. Am. Chem. Soc.* **1994**, *116*, 11898−11914.
(12) Stephens, P. J.; Jollie, D. R.; Warshel, A. *Chem. Rev.* 1996, *96*, 2491−2513.
(13) Banci, L.; Bertini, I.; Savellini, G. G.; Luchinat, C. *Inorg. Chem.* 1996, *35*, 4248−4253.
(14) Beck, B. W.; Xie, Q.; Ichiye, T. *Biophys. J.* **2001**, *81*, 601−613.
(15) Noodleman, L.; Case, D. A. In *Advances in Inorganic Chemistry;* Cammack, R., Ed.; Academic Press: San Diego, CA, 1992; Vol. 38, pp 423−470.

10.1021/ja0211104 CCC: $25.00

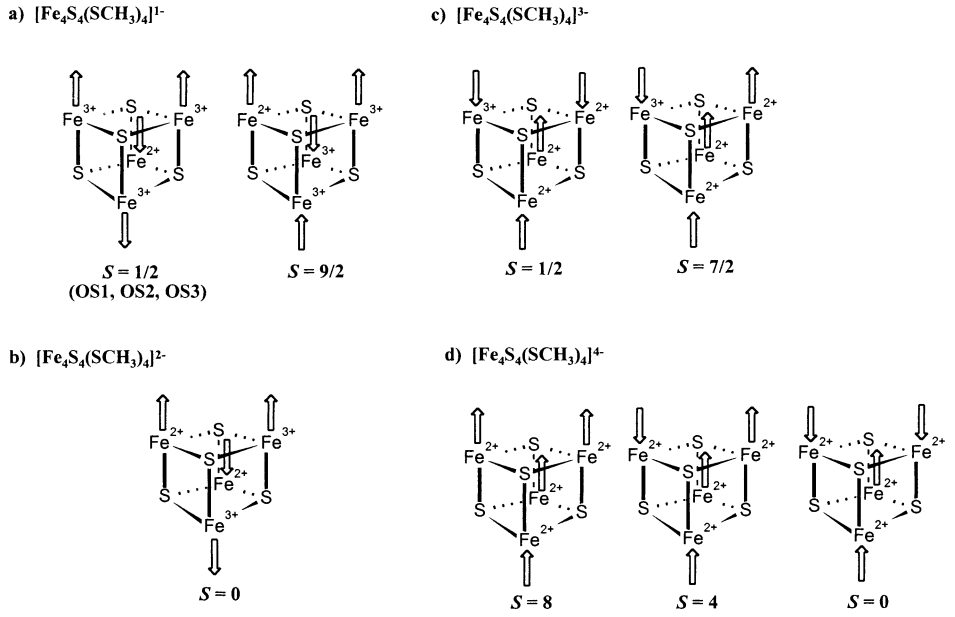

Figure 1. Summary of the oxidation and spin states investigated in this study. The majority spin electrons are referred to as open arrows, and iron atoms are referred to by their formal charges.

treatment of spin-coupled systems that formally contain a large number of unpaired electrons is necessary in density functional theory (DFT). In most Fe_4S_4 systems, the iron sites are high spin and antiferromagnetically coupled, yet the total spin of low-lying excited states or the composition of total spin in the ground state with respect to the subunit contributions is not always evident. To discuss trends in Fe_4S_4 clusters, it is essential to be able to describe weak antiferromagnetic coupling at the same level of theory as strong metal−metal and metal−ligand bonding. This is possible in DFT by making use of the broken symmetry concept of electronic structure (BS), which treats weakly interacting electrons in a physically realistic manner. This spin-unrestricted approach has been applied with considerable success in the study of a variety of inorganic and biologically relevant species. For a more detailed description and the success in reproducing experimental results utilizing the broken symmetry method, the reader is referred to previous work.[11,15,18−22] In particular, eight years ago, we used techniques similar to those reported here to study midpoint reduction potentials of a few iron−sulfur clusters.[11] This paper extends the earlier work in several directions: usage of geometry-optimized structures (rather than assumed geometries), consideration of both protein and homogeneous solution environments, and extension of the results to the 0 and 4^- cluster oxidation states that were not known at the time of the earlier work.

It had been previously established that the Fe_4S_4 clusters in proteins exist primarily in three oxidation states.[23] Studies of the Fe protein of nitrogenase have provided evidence supporting the existence of an unprecedented all-ferrous cluster, and synthetic efforts have resulted in an all-ferric cluster, increasing the number of known oxidation states of these cubane clusters to five. In this study, the results of density functional geometry optimizations on model clusters of the form $[Fe_4S_4(SCH_3)_4]^{0,1-,2-,3-,4-}$ are presented (Scheme 1). Combined DFT and continuum solvent techniques are used to calculate reduction potentials of these clusters in solvent and are compared with the observed midpoint potentials of synthetic clusters. The geometry and associated charges of the model Fe_4S_4 clusters were then used to calculate the midpoint potentials in several proteins, including high potential iron proteins (HiPIPs), ferredoxin (Fd) proteins, photosystem I (PS I), and the Fe protein of nitrogenase (Fe protein).

Scheme 1

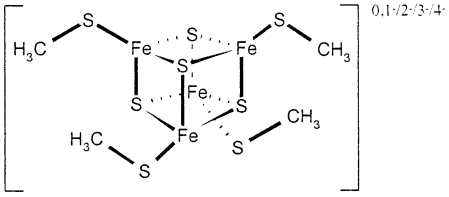

2. Geometries and Spin States

Geometry optimizations, unless otherwise noted in Table 1, have been performed with C_{2v} symmetry. The results of geometry optimizations on each system employing the spin-coupling schemes outlined in Figure 1 for each system and their associated solvation energies are discussed later. Since the 1^-, 2^-, and 3^- oxidation states have been discussed in our earlier work,[11] we discuss here the effects of geometry optimization, which is new. A more detailed description is given for the DFT results for the 4^- oxidation state, which had not been described previously. Since very little is known about the all-ferric oxidation state of the Fe_4S_4 cubanes, we only investigated the $S = 0$ spin state of this model cluster and predict its associated cluster geometry.

(16) Seminaro, J. M., Ed. *Recent Developments and Applications of Modern Density Functional Theory*; Elsevier: Amsterdam, 1996.
(17) Ziegler, T. *Chem. Rev.* **1991**, *91*, 651−667.
(18) Noodleman, L.; Peng, C. Y.; Case, D. A.; Mouesca, J.-M. *Coord. Chem. Rev.* **1995**, *144*, 199−244.
(19) Li, J.; Nelson, M. R.; Peng, C. Y.; Bashford, D.; Noodleman, L. *J. Phys. Chem. A* **1998**, *102*, 6311−6324.
(20) Li, J.; Beroza, P.; Noodleman, L.; Case, D. A. In *Molecular Modeling and Dynamics of Bioinorganic Systems;* Banci, L. a..C., P., Ed.; Kluwer Academic Publishers: The Netherlands, 1997; pp 279−306.
(21) Konecny, R.; Li, J.; Fisher, C. L.; Dillet, V.; Bashford, D.; Noodleman, L. *Inorg. Chem.* **1999**, *38*, 940−950.
(22) Fisher, C. L.; Chen, J.-L.; Li, J.; Bashford, D.; Noodleman, L. *J. Phys. Chem. B* **1996**, *100*, 13498−13505.
(23) Carter, C. W. In *Iron−Sulfur Proteins;* Lovenberg, W., Ed.; Academic Press: New York, 1977; pp 157−204.

Table 1. Geometrical Data of the Optimized Model Clusters[g]

		calculated			experiment[f]		
system	symmetry	Fe–Fe, (Å)	Fe–S*, (Å)	Fe–S, (Å)	Fe–Fe, (Å)	Fe–S*, (Å)	Fe–S, (Å)
$[Fe_4S_4(SCH_3)_4]^0$	C_{2v}	2.610 (×2)	2.216 (×8)	2.237 (×4)			
$S = 0$		2.674 (×4)	2.220 (×4)				
$[Fe_4S_4(SCH_3)_4]^{1-}$ [a]	C_{2v}	2.616	2.272 (×8)	2.237 (×4)			
$S = 1/2$		2.783	2.220 (×4)				
		2.705 (×4)					
$[Fe_4S_4(SCH_3)_4]^{1-}$ [b]	C_{2v}	2.699	2.274 (×8)	2.236 (×4)	2.754	2.271 (×4)	2.209 (×2)
$S = 1/2$		2.674	2.217 (×4)		2.724	2.279 (×4)	2.204 (×2)
		2.714 (×4)			2.740 (×4)	2.234 (×4)	
$[Fe_4S_4(SCH_3)_4]^{1-}$ [c]	C_{2v}	2.946	2.302 (×8)	2.245 (×4)			
$S = 1/2$		2.960	2.201 (×4)				
		2.750 (×4)					
$[Fe_4S_4(SCH_3)_4]^{1-}$	C_1	2.829	2.318 (×8)	2.254 (×4)			
$S = 9/2$		2.769[d]	2.315 (×4)				
		2.798 (×4)					
$[Fe_4S_4(SCH_3)_4]^{2-}$	C_{2v}	2.809 (×2)	2.332 (×8)	2.302 (×4)	2.775 (×2)	2.310 (×8)	2.251 (×4)
$S = 0$		2.741 (×4)	2.224 (×4)		2.733 (×4)	2.241 (×4)	
$[Fe_4S_4(SCH_3)_4]^{3-}$							
$S = 1/2$	C_{2v}	2.781	2.346 (×8)	2.383 (×4)	2.743 (×2)	2.291 (×8)	2.295 (×4)
		2.813	2.267 (×4)		2.743 (×4)	2.352 (×4)	
		2.777 (×4)					
$S = 7/2$	C_1	2.796[d]	2.337 (×8)	2.368 (×3)			
		2.638	2.327 (×4)	2.413			
		2.755 (×4)					
$[Fe_4S_4(SCH_3)_4]^{4-}$							
$S = 4$[e]	C_1	2.866[d]	2.378 (×8)	2.410 (×2)			
		2.626	2.357 (×4)	2.542 (×2)			
		2.756 (×4)					
$S = 0$	C_1	2.805 (×2)	2.366 (×8)	2.382 (×4)			
		2.851 (×4)	2.308 (×4)				
$S = 8$	C_1	2.607	2.384 (×8)	2.562 (×4)			
		2.626	2.447 (×4)				
		2.822 (×4)					

[a] OS1 state. [b] OS2 state. [c] OS3 state. [d] Distance of intralayer antiferromagnetic pair. [e] $S = 4$ refers to the BS1 state, $S = 0$ refers to the BS2 state, and $S = 8$ refers to the HS state. [f] Values from refs 70−72. [g] Some values have been averaged.

2.1. $[Fe_4S_4(SCH_3)_4]^{2-}$. The results of the geometry optimization of the $S = 0$ BS ground state of this model system (Figure 1b) are presented in Table 1. This is the simplest and best-defined oxidation state of the Fe_4S_4 clusters. The Fe−Fe, Fe−S* (Fe to bridging S atom), and Fe−S (Fe to organic S atom) distances shown deviate only slightly from those seen in some of the original model complexes,[9,11] although in general the geometry-optimized structure is slightly expanded compared to crystal structures. For example, the intralayer Fe−Fe geometry-optimized distances are calculated to be 0.034 Å longer and the interlayer Fe−Fe distances are 0.008 Å longer than the experimental structure. Similarly, the Fe−S* and Fe−S average distances are 0.010 and 0.051 Å longer than experiment, respectively. Overall, the calculated and observed structural parameters are in quite good agreement, lending support to our use of calculated geometries for other oxidation states, where the experimental structures are less clear.

We repeated the geometry optimization procedure using the COSMO solvation model, as implemented in ADF2000 with dielectric 37 and a probe radius of 3.7 Å to represent the solvent dimethylformamide. Here, the gas-phase electron−electron repulsion was screened by the solvent, as expected, and somewhat improved geometries were obtained. The Fe−Fe intralayer distances were 2.748 (×2) Å, while the Fe−Fe interlayer distances were 2.704 (×4) Å. The Fe−S* COSMO geometry-optimized distances were 2.334 (×8) Å and 2.274 (×4), and the Fe−S distances were 2.231 (×4). These COSMO geometry-optimized distances are slightly shorter than the gas-phase results (Table 1) and in very good agreement with the experimental model cluster data. Additional geometry optimizations using COSMO are planned for the clusters investigated in this work.

2.2. $[Fe_4S_4(SCH_3)_4]^{1-}$. Previous calculations on this model system (Figure 1a) were performed on three electronic orbital configurations of the $S = 1/2$ spin ground states designated OS1, OS2, and OS3.[11,24] The OS3 state is generated by removing an electron from the σ-bonding orbital of one Fe−Fe pair of the 2^- cluster, resulting formally in an Fe^{3+}−Fe^{3+} pair and an Fe^{2+}−Fe^{3+} pair. The OS1 and OS2 configurations are generated from OS3 via spin forbidden transitions and are described by identical spin algebra (see Appendix and ref 11 for a detailed explanation). The geometric data for these cluster systems are presented in Table 1. OS1 and OS2 display cluster geometries that are compressed relative to experiment, while OS3 has an expanded geometry, as does the high energy $S = 9/2$ state. The OS1, OS2, and OS3 substates display somewhat different geometries from one another, while their gas-phase energies lie within 0.14 eV of each other (Table 2). The OS1 state has

(24) Noodleman, L. *Inorg. Chem.* **1988**, *27*, 3677−3679.

Table 2. Calculated Raw Energies of the Model Fe_4S_4 Clusters (in eV)

system	$E_{BS,gas}$	E_{PB} $\epsilon = 37$, radius 1.4 Å	E_{PB} $\epsilon = 37$, radius 3.7 Å	E_{PB} $\epsilon = 80$, radius 1.4 Å
$[Fe_4S_4(SCH_3)_4]^0$	−147.93	−1.71	−1.69	−1.74
$[Fe_4S_4(SCH_3)_4]^{1-}$ [a]	−151.12	−2.35	−2.01	−2.43
$[Fe_4S_4(SCH_3)_4]^{1-}$ [b]	−151.08	−2.19	−2.03	−2.23
$[Fe_4S_4(SCH_3)_4]^{1-}$ [c]	−150.98	−2.16	−2.01	−2.20
$[Fe_4S_4(SCH_3)_4]^{1-}$				
$S = {}^9/_2$	−150.31	−2.19	−2.05	−2.23
$[Fe_4S_4(SCH_3)_4]^{2-}$	−150.95	−6.81	−6.60	−6.92
$[Fe_4S_4(SCH_3)_4]^{3-}$				
$S = {}^1/_2$	−146.74	−14.48	−14.01	−14.70
$S = {}^7/_2$	−146.86	−14.43	−13.97	−14.70
$[Fe_4S_4(SCH_3)_4]^{4-}$				
$S = 4$	−139.72	−24.65	−24.13	−25.04
$S = 0$	−139.74	−24.33	−23.80	−24.71
$S = 8$	−139.34	−24.76	−24.09	−25.15

[a] OS1 state. [b] OS2 state. [c] OS3 state.

the lowest gas-phase and solvation energies in this series (Table 3), as in our earlier calculations.[11] It should be noted that since OS1, OS2, and OS3 are nearly isoenergetic, a physical or quantum mixture may occur in the HiPIP redox states for some proteins and synthetic systems. The gas-phase energy of the hypothetical $S = {}^9/_2$ cluster is significantly higher than the energies of the other 1^- clusters (0.67−0.81 eV), suggesting this state is significantly destabilized relative to the $S = {}^1/_2$ states.

As we have discussed earlier, the OS3 broken symmetry state is not a good model for the true ground state because of spin canting.[11] This is likely to cause its geometry to be poor for some Fe−Fe distances, as seen in Table 1. This spin-canting problem should be less severe for OS1 and OS2, although here the calculated geometries are somewhat contracted relative to experiment. A more complete analysis would probably be required to obtain geometries as good as those obtained for the 2^- cluster, which has a much simpler spin-coupling scheme.

2.3. $[Fe_4S_4(SCH_3)_4]^{3-}$. Two low-lying ground states at this oxidation state of the Fe_4S_4 cluster were examined here: $S = {}^1/_2$ and $S = {}^7/_2$. The BS $S = {}^1/_2$ state reported here is that of OC2.[11] The geometry of this spin state is slightly expanded relative to the experimentally determined cluster. This spin state also displays a 4:1:1 pattern of Fe−Fe distances, which may also be considered an approximate 5:1 pattern, while a definite 4:1:1 pattern of Fe−Fe distances is seen in the $S = {}^7/_2$ spin-coupling mode. For the $S = {}^7/_2$ state, the short intralayer Fe−Fe distance arises primarily because of overlap of the $d(xz)$ and $d(x^2-y^2)$ metal-based orbitals, resulting in a σ-type interaction. The long Fe−Fe intralayer distance is characterized by overlap of the metal-based d orbitals in a π-type fashion. This layer contains iron atoms that are antiferromagnetically coupled with one another, such that one iron in the cluster system is unique. When the gas-phase broken symmetry energy is corrected by spin projection (*vide infra*) and the cluster is placed in a dielectric medium of 37, the $S = {}^1/_2$ spin state appears slightly below that of the $S = {}^7/_2$ spin state, as detailed in the Appendix.

2.4. $[Fe_4S_4(SCH_3)_4]^{4-}$. Prior to the discovery of the $[Fe_4S_4]^0$ cluster in the Fe protein of nitrogenase, Fe_4S_4 clusters in proteins were only believed to function at the $[Fe_4S_4]^{3+/2+}$ and $[Fe_4S_4]^{2+/1+}$ redox levels.[23] Since this discovery, it has been suggested[25] that the Fe_4S_4 cluster in the Fe protein incorporates three oxidation states (two redox couples) during its reduction ($[Fe_4S_4]^{2+/1+}$ and $[Fe_4S_4]^{1+/0}$). This fluctuation in oxidation states may play a role in the reduction of the MoFe protein, the protein component in which nitrogen binding and fixation occurs.

Model Fe_4S_4 complexes with sulfur-containing ligands at the all-ferrous level are not yet available, which precludes a direct

Table 3. Calculated Charges and Net Spin Densities for $[Fe_4S_4(SCH_3)_4]^{3-,2-,1-}$ [a]

	3−			2−	1−		
atom	$S = {}^1/_2$	$S = {}^7/_2$			OS 1	OS2	OS3
				a. ESP charges			
Fe_{ox}	+0.743 (×2)	+0.634	+0.727	+0.642 (×2)	+0.521 (×2)	+0.533 (×2)	+0.549 (×2)
Fe_{red}	+0.728 (×2)	+0.665	+0.674	+0.635 (×2)	+0.545 (×2)	+0.545 (×2)	+0.536 (×2)
S^*_{ox}	−0.749 (×2)	−0.656	−0.644	−0.584 (×2)	−0.399 (×2)	−0.423 (×2)	−0.422 (×2)
S^*_{red}	−0.745 (×2)	−0.632	−0.815	−0.580 (×2)	−0.436 (×2)	−0.428 (×2)	−0.432 (×2)
S_{ox}	−0.711 (×2)	−0.702	−0.774	−0.574 (×2)	−0.402 (×2)	−0.412 (×2)	−0.419 (×2)
S_{red}	−0.743 (×2)	−0.757	−0.770	−0.571 (×2)	−0.443 (×2)	−0.430 (×2)	−0.424 (×2)
CH_{3ox}	+0.018 (×2)	+0.009	+0.029	+0.016 (×2)	+0.059 (×2)	+0.062 (×2)	+0.065 (×2)
CH_{3red}	+0.040 (×2)	+0.009	+0.024	+0.016 (×2)	+0.056 (×2)	+0.050 (×2)	+0.047 (×2)
				b. Mulliken charges			
Fe_{ox}	+0.541 (×2)	+0.547	+0.536	+0.504 (×2)	+0.433 (×2)	+0.445 (×2)	+0.486 (×2)
Fe_{red}	+0.525 (×2)	+0.531	+0.531	+0.503 (×2)	+0.482 (×2)	+0.470 (×2)	+0.470 (×2)
S^*_{ox}	−0.669 (×2)	−0.652	−0.636	−0.550 (×2)	−0.418 (×2)	−0.425 (×2)	−0.464 (×2)
S^*_{red}	−0.660 (×2)	−0.651	−0.746	−0.550 (×2)	−0.438 (×2)	−0.432 (×2)	−0.436 (×2)
S_{ox}	−0.645 (×2)	−0.616	−0.662	−0.546 (×2)	−0.403 (×2)	−0.411 (×2)	−0.416 (×2)
S_{red}	−0.667 (×2)	−0.663	−0.654	−0.545 (×2)	−0.438 (×2)	−0.429 (×2)	−0.440 (×2)
CH_{3ox}	+0.040 (×2)	+0.043	+0.025	+0.093 (×2)	+0.143 (×2)	+0.146 (×2)	+0.153 (×2)
CH_{3red}	+0.035 (×2)	+0.041	+0.028	+0.093 (×2)	+0.138 (×2)	+0.182 (×2)	+0.147 (×2)
				c. Net Spin Densities			
Fe_{ox}	+3.286 (×2)	−3.234.	+3.231	−3.127 (×2)	−2.448 (×2)	−2.469 (×2)	+3.255 (×2)
Fe_{red}	−3.005 (×2)	+3.249	+3.198	+3.127 (×2)	+2.920 (×2)	+2.895 (×2)	−3.006 (×2)
S^*_{ox}	+0.152 (×2)	+0.013	−0.052	−0.010 (×2)	+0.063 (×2)	+0.078 (×2)	+0.075 (×2)
S^*_{red}	+0.032 (×2)	+0.034	+0.422	+0.011 (×2)	−0.016 (×2)	+0.006 (×2)	+0.083 (×2)
S_{ox}	+0.096 (×2)	−0.116	+0.068	−0.152 (×2)	−0.199 (×2)	−0.196 (×2)	+0.291 (×2)
S_{red}	−0.061 (×2)	+0.072	+0.074	+0.152 (×2)	+0.178 (×2)	+0.184 (×2)	−0.201 (×2)
CH_{3ox}	+0.007 (×2)	−0.004	−0.006	−0.015 (×2)	−0.018 (×2)	−0.018 (×2)	+0.023 (×2)
CH_{3red}	−0.006 (×2)	+0.014	+0.015	+0.015 (×2)	+0.019 (×2)	+0.019 (×2)	−0.021 (×2)

[a] The 2^- cluster is the reference state.

structural comparison with calculated values. However, structural comparisons with available data on the Fe protein of nitrogenase are possible. The Fe protein has been examined experimentally by EXAFS,[26] Mössbauer and EPR spectroscopy,[27,28] and X-ray crystallography.[29−32] The best fit to the EXAFS data implies a 2:4 long:short pattern of Fe−Fe distances (i.e., ratio of one long, 2.77 Å, to two short, 2.52 Å), resulting in a tetragonally compressed $[Fe_4S_4]^0$ cluster. The unusually short Fe−Fe distance indicated by the EXAFS data presents the intriguing possibility of some metal−metal bonding in the $[Fe_4S_4]^0$ cluster. Mössbauer and EPR studies indicate an $S = 4$ spin state is present with one Fe site clearly distinguishable within the cluster.[27] The authors suggested that the presence of the unique iron may be of fundamental importance to the chemistry of the all-ferrous cluster.[27,28] Several crystallographic structures of the Fe protein have been solved, with the cluster in the 1g5p structure[29] most likely to be in the all-ferrous state. The resolution (2.25 Å) of the all-ferrous Fe protein is not accurate enough to provide reliable cluster geometries, and the various Fe protein crystal structures vary considerably. Thus, the relationship between the experimental results for the spectroscopy and geometry of the Fe_4S_4 clusters in the all-ferrous state is not readily obvious.

Three independent cases of spin-coupling alignments associated with the iron atoms were considered (Figure 1d). These are (1) all Fe^{2+} majority spin vectors aligned in parallel (HS, $S = 8$), (2) one Fe^{2+} spin vector flipped relative to the other three sites (BS1, $S = 4$), and (3) two up spin vectors and two down spin vectors (BS2, $S = 0$). Strong evidence for the existence of the BS1 state in the Fe protein has been provided by Mössbauer studies where a unique iron site is established, presumably generated because of environmental or geometric asymmetries in the protein. Here, the "dimer of dimers" model is no longer valid, and the cluster symmetry is lowered from a pairwise equivalence (2:2) to a model in which a single site is differentiated from the others. Structural properties of these three spin states are presented in Table 1.

The Fe−Fe distances of the HS state display a 4:2 long/short pattern. In this state, the short intralayer Fe−Fe distances (2.607 and 2.626 Å) arise because of overlap of the metal-based $d(x^2-y^2)$ orbitals (of minority spin) in one layer, while, in the other layer, the overlap is between $d(z^2)$ orbitals (data not shown). The $d(x^2-y^2)$ overlap is σ-type and short bond distances result. The longer interlayer Fe−Fe distances (2.822 Å) appear to be primarily due to weaker π-type interactions between the d orbitals.

The BS2 state displays a 4:2 long to short pattern, with the interlayer Fe−Fe distances longer than the intralayer Fe−Fe distances. Here, overlap of the $d(xz)$ orbitals in one layer and the $d(xy)$ orbitals in the second layer occurs, giving rise to a σ-type interaction within the Fe−Fe intralayer distances. A π-type interaction can be seen in the Fe−Fe interlayer distances, although to a lesser extent than in the HS state, and longer interlayer Fe−Fe distances. Finally, in the BS1 state, the layer (Fe1−Fe2) containing the unique iron (Fe1) exhibits a mixed π,δ-type interaction with little overlap of the $d(xz)$, $d(yz)$, and $d(x^2-y^2)$ orbitals (Figure 2), resulting in a long Fe−Fe distance. In contrast, there is significant overlap between the metal-based $d(xz)$, $d(xy)$, and $d(z^2)$ orbitals, giving a σ-type interaction and a short Fe3−Fe4 intralayer distance. Moderate overlap between the metal-based orbitals in a σ- and π-type manner occurs such that the interlayer Fe−Fe distances are comparable to the calculated interlayer Fe−Fe distances of the $[Fe_4S_4]^{2+}$ and $[Fe_4S_4]^{1+}$ model clusters. These distances also compare well to the interlayer Fe−Fe distances determined experimentally.[26] Thus, on the basis of the calculated Fe−Fe distances in this cluster system, a 4:1:1 pattern appears, similar to that observed in the calculated $S = {}^7/_2$ state of the $[Fe_4S_4]^{1+}$ cluster (*vide supra*). This comparable pattern is understandable, as the $S = {}^7/_2$ state of the $[Fe_4S_4]^{1+}$ cluster results because of a loss of an electron from the unique iron (loss of a minority spin up electron). The calculated distances for the BS1 state are within the 95% confidence interval of the EXAFS fit data,[26] although the pattern of distances deviates somewhat from the experimental fit. The HS and BS2 Fe−Fe distances are also within the experimental error of the EXAFS fit data. Table 2 displays the gas-phase and solvation energies calculated for the HS, BS1, and BS2 states. The BS2 and BS1 states were found to have the lowest gas-phase energies (for $\epsilon_s = 37$, radius 3.7 Å); however, when the gas-phase and solvation energies are combined, the $S = 4$ (BS1) spin state is lowest in total energy (Table 2).

A simplified energy level diagram for BS1 is shown in Figure 2. The distance between the antiferromagnetic Fe−Fe pair (Fe1−Fe2) was calculated to be 2.866 Å, while that of the ferromagnetic pair (Fe3−Fe4) was 2.626 Å (Table 1). Isosurface contour plots of notable molecular orbitals associated with this BS state are also incorporated in this figure. A 3:1 site spin pattern having a significant delocalization of minority spin is evident. This approximate pattern was suggested on the basis of Mössbauer and EPR studies of the $S = 4$ spin state of the Fe protein from *Azotobacter vinelandii*.[27,28] The isosurface plot of the 76α molecular orbital associated with the unique iron (Fe1) shows that no effective electron delocalization pathway exists (for the minority spin up electron of the unique iron). Therefore, little or no metal−metal interaction between Fe1 and the remaining iron atoms in the cluster occurs. This is in contrast to that observed for the HS state, where, as a result of the parallel alignment of all the iron site spin vectors, delocalization pathways exist between all iron minority spin electrons (data not shown). Isosurface plots of the 66β, 67β, and 68β molecular orbitals show that the minority spin densities from these are higher for sites Fe2, Fe3, and Fe4 and that delocalization pathways clearly exist between minority spin down electrons of these atoms, indicating some form of metal−metal interaction.

3. Charge and Spin Distributions

3.1. ESP and Mulliken Charges. The results of the ESP and Mulliken charges for the geometry-optimized Fe_4S_4 clusters examined in this study are given in Tables 3 and 4. The ESP charges are significantly larger than those determined by the Mulliken charge analysis, such that the calculated polarity of

(25) Watt, G. D.; Reddy, K. R. N. *J. Inorg. Biochem.* **1994**, *53*, 281−294.
(26) Musgrave, K. B.; Angrove, H. C.; Burgess, B. K.; Hedman, B.; Hodgson, K. O. *J. Am. Chem. Soc.* **1998**, *120*, 5325−5326.
(27) Yoo, S. J.; Angrove, H. C.; Burgess, B. K.; Hendrich, M. P.; Munck, E. *J. Am. Chem. Soc.* **1999**, *121*, 2534−2545.
(28) Angrove, H. C.; Yoo, S. J.; Burgess, B. K.; Munck, E. *J. Am. Chem. Soc.* **1997**, *119*, 8730−8731.
(29) Strop, P.; Takahara, P. M.; Chiu, H.-J.; Angrove, H. C.; Burgess, B. K.; Rees, D. C. *Biochemistry* **2001**, *40*, 651−656.
(30) Schlessman, J. L.; Woo, D.; Joshua-Tor, L.; Howard, J. B.; Rees, D. C. *J. Mol. Biol.* **1998**, *280*, 669−685.
(31) Georgiadis, M. M.; Komiya, H.; Chakrabarti, P.; Woo, D.; Kornuc, J. J.; Rees, D. C. *Science* 1992, *257*, 1653−1659.
(32) Jang, S. B.; Seefeldt, L. C.; Peters, J. W. *Biochemistry* **2000**, *39*, 14745−14752.

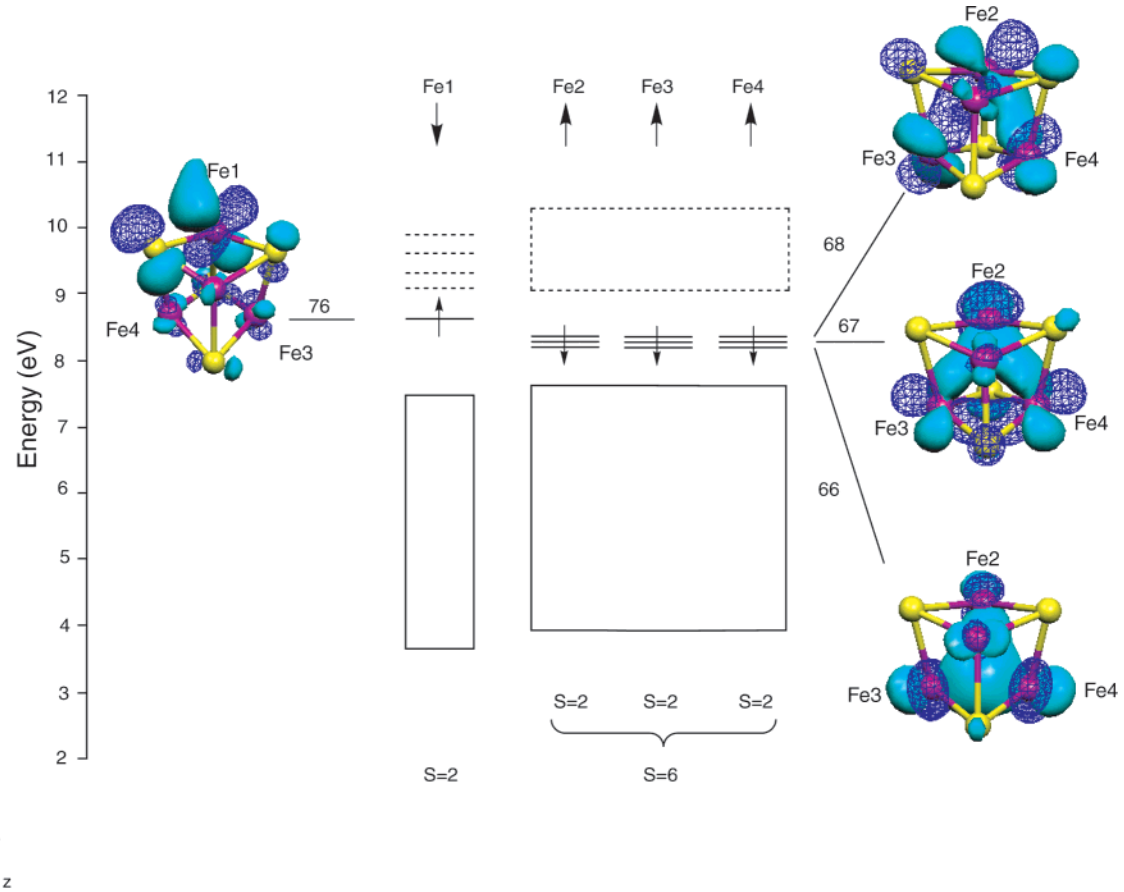

Figure 2. Simplified orbital energy diagram and isosurface contour plots of the $S = 4$ spin state of the $[Fe_4S_4(SCH_3)_4]^{4-}$ cluster. Iron atoms are magenta in color, while sulfur atoms are in yellow; only the core cluster atoms are shown. Large arrows represent majority spin electrons, while small arrows refer to minority spin electrons. Unoccupied orbitals are displayed as dashed lines, while occupied orbitals are presented as solid lines. The minority spin high lying orbitals shown have substantial Fe 3d character. Pure, ligand-based orbitals (S, C, and H) have been omitted for clarity. The $\bar{4}$ axis is *x*, while the Fe1−Fe2 bond axis is *y* and the Fe3−Fe4 bond axis is *z*. The figure was prepared using MOLEKEL.[81]

Table 4. Calculated Charges and Net Spin Densities for $[Fe_4S_4(SCH_3)_4]^{4-}$

atom	$S = 8$		$S = 4$		$S = 0$	
			a. ESP charges			
$Fe_{1,2}$	+0.770	+0.744	+0.772	+0.754	+0.782	+0.724
$Fe_{3,4}$	+0.812	+0.759	+0.777	+0.708	+0.780	+0.733
$S^*_{5,6}$	−0.895	−0.855	−0.852	−0.812	−0.836	−0.788
$S^*_{7,8}$	−0.925	−0.871	−0.820	−0.885	−0.848	−0.775
$S_{9,10}$	−0.866	−0.839	−0.869	−0.869	−0.867	−0.859
$S_{11,12}$	−0.849	−0.851	−0.859	−0.877	−0.869	−0.862
$CH_{3(13,14)}$	−0.016	−0.044	−0.082	−0.026	−0.089	−0.072
$CH_{3(15,16)}$	−0.037	−0.035	−0.040	−0.019	−0.085	−0.074
			b. Mulliken charges			
$Fe_{1,2}$	+0.582	+0.571	+0.554	+0.582	+0.561	+0.569
$Fe_{3,4}$	+0.570	+0.573	+0.555	+0.559	+0.561	+0.569
$S^*_{5,6}$	−0.802	−0.808	−0.767	−0.766	−0.780	−0.749
$S^*_{7,8}$	−0.812	−0.797	−0.766	−0.831	−0.781	−0.749
$S_{9,10}$	−0.752	−0.766	−0.689	−0.724	−0.692	−0.690
$S_{11,12}$	−0.779	−0.768	−0.758	−0.752	−0.690	−0.688
$CH_{3(13,14)}$	−0.014	−0.002	−0.118	−0.037	−0.115	−0.102
$CH_{3(15,16)}$	+0.006	−0.002	−0.015	−0.016	−0.116	−0.105
			c. net spin densities			
$Fe_{1,2}$	+3.501	+3.495	−3.097	+3.356	−3.191	−3.186
$Fe_{3,4}$	+3.511	+3.503	+3.664	+3.357	+3.193	+3.188
$S^*_{5,6}$	+0.428	+0.410	+0.095	+0.166	−0.086	−0.083
$S^*_{7,8}$	+0.426	+0.399	+0.108	+0.421	+0.086	+0.083
$S_{9,10}$	+0.059	+0.061	−0.068	+0.058	−0.060	−0.061
$S_{11,12}$	+0.060	+0.058	+0.042	+0.041	+0.061	+0.061
$CH_{3(13,14)}$	+0.023	+0.023	+0.012	+0.012	+0.090	+0.070
$CH_{3(15,16)}$	+0.023	+0.021	+0.022	+0.017	−0.077	−0.073

the Fe−S bonds is greater when evaluated by the ESP method. A general trend of increasing positive charge associated with the iron atoms and progressively more negative charges associated with the sulfur atoms can be seen as the clusters become more reduced in both methods. Also, both the ESP and Mulliken charges increase on the Fe_{ox} pair from the OS1 or OS2 substate to the OS3 substate in the $[Fe_4S_4]^{3+}$ system. The data suggest the ESP charges display only a small degree of sensitivity to the electronic state and associated geometry in the 3^+ cluster. These results are similar to those obtained in previous calculations on these systems[11] and provide an extended collection of charges that could also be used for molecular mechanical modeling of iron−sulfur cubanes.

3.2. Spin Populations. The net spin populations (which include $s + p + d$ contributions) for the systems of interest were determined using a Mulliken population analysis, and the results are shown in Tables 3 and 4. It can been see that a general decrease in spin population on iron occurs for a given cluster as the formal oxidation state is reduced from Fe^{3+} to $Fe^{2.5+}$ to Fe^{2+}, as found in previous studies.[11] It should be noted that deviations from this trend occur within a given oxidation state; however, these deviations are likely due to spin rearrangements that accompany spin transitions. For example, in the case of the 1^- clusters, the OS3 substate has a higher spin population (with an average of 3.131), while the average spin populations for OS1 and OS2 are 2.684 and 2.682, respectively. Here, the variation is largely due to spin transitions in the diferric (Fe_{ox}) pair, while the mixed valence pair is largely unaffected (see

Table 5. Comparison of Calculated and Experimental Redox Potentials of Model Systems (in eV).

	($\epsilon = 80$)		($\epsilon = 37$)			
system	1994 DFT[e]	$E°_{calc}$[g]	1994 DFT[e]	$E°_{calc}$[g] (radius 1.4 Å)	$E°_{calc}$[g] (radius 3.7 Å)	experimental[f]
$[Fe_4S_4(SCH_3)_4]^{1-/0}$ $S = 0$	nd	+0.16	nd	+0.13	+0.11	+0.34
$[Fe_4S_4(SCH_3)_4]^{2-/1-\,a}$ $S = {}^1/_2$	+0.05	−0.11	−0.02	−0.14	−0.01	+0.10
$[Fe_4S_4(SCH_3)_4]^{2-/1-\,b}$ $S = {}^1/_2$	+0.38	+0.16	+0.32	−0.04	+0.04	+0.10
$[Fe_4S_4(SCH_3)_4]^{2-/1-\,c}$ $S = {}^1/_2$	+0.63	+0.14	+0.56	+0.07	+0.02	+0.10
$[Fe_4S_4(SCH_3)_4]^{2-}$ $S = 0$	ref					
$[Fe_4S_4(SCH_3)_4]^{3-/2-}$						
$S = {}^1/_2$	−1.56	−0.89	−1.45	−1.01	−1.26	−1.1
$S = {}^7/_2$	nd	−0.90	nd	−1.07	−1.32	nd
$[Fe_4S_4(SCH_3)_4]^{4-/3-}$						
$S = 4$[d]	nd	−1.42	nd	−1.58	−1.64	−1.27 to −1.61
$S = 0$[d]	nd	−1.70	nd	−1.86	−1.93	nd
$S = 8$[d]	nd	−1.71	nd	−1.88	−2.08	nd

[a] OS1 state. [b] OS2 state. [c] OS3 state. [d] Reduction potentials calculated with respect to the $S = {}^1/_2$ state of $[Fe_4S_4(SCH_3)_4]^{3-}$. [e] Calculated reduction potentials taken from ref 11. [f] All experimental reduction potentials are taken from refs 9, 36, and 82. [g] For this work, see eq 1. Ref, reference state; nd, not determined.

Appendix). Within a given cluster, with the exception of OS1, OS2 (1^-), the higher oxidation state sites typically have larger spin densities, as expected. Upon one-electron reduction, much of the electron density from the additional electron is redistributed to other positions, primarily to the sulfur atoms. The amount of metal−metal and metal−ligand covalency can be approximately gauged when the spin population ratios (ratio of calculated to formal values) are examined. Smaller percentages indicate greater metal−ligand covalency and, perhaps, enhanced metal−metal interactions. The spin population ratios for the 1^- cluster range from 54 to 66%, 69% for the 2^- state, from 72 to 81% for 3^-, and from 77 to 88% for 4^-. Overall, the ratios show a significant amount of metal−ligand covalency, with the greatest found in the 1^- cluster.

4. Reduction Potentials

The spin-coupling and electron delocalization terms exert a large and systematic effect on observed reduction potentials of iron−sulfur clusters. This can be seen in the trends of reduction potentials for both synthetic complexes in solvent and in proteins. The calculation of the gas-phase electronic structure in combination with continuum dielectric methods has been shown to provide reasonably good estimates of these effects.[11,19−21,33−35] Calculations of model clusters in solvent were performed according to the following equation: E^0_{calc} = IP(red) + ΔE_{PB} + $\Delta\Delta E_{spin}$ + ΔSHE (eq 1 in Computational Methods). The IP(red) term represents the difference in the gas-phase ionization potentials between the reduced and oxidized species, which is added to the solvation energy difference between these two species(ΔE_{PB}). The spin projection correction ($\Delta\Delta E_{spin}$, see Appendix) is added to this value, and the sum is referenced to the standard hydrogen electrode (ΔSHE), to provide the calculated standard reduction potential. The solvent region, for the calculation of E_{PB}, is assigned as the bulk dielectric constant for the solvent of interest, while that of the quantum region is assigned a value of one. Two different probe radii (1.4 and 3.7 Å) were used to calculate the reduction potentials of these model clusters in $\epsilon_s = 37$ to compare the current results to previous calculations and to approximate the radius of the solvent in which the synthetic clusters were placed, respectively. Calculations of the reduction potential of the clusters in their respective proteins were performed according to eq 1 as well and incorporate an additional dielectric constant region corresponding to the protein which is assigned a value of four. Here, E_{PB} contains both a reaction field term and a protein field term.[19−21] Additional details of these calculations are given in the Computational Methods section. Values determined for the model clusters in water and acetonitrile (or DMF) are discussed first.

4.1. Reduction Potentials in Solvent. Reduction potentials calculated in the solvent reaction field for each model cluster system are shown in Table 5. These results are compared to previous calculations and to experimentally determined reduction potentials. The results of the midpoint potential calculations presented here more closely approximate the experimentally determined potentials for model systems than in previous work.[11] The primary reason for this difference is likely due to the effect of geometry optimization, although the exchange-correlation potential used in the current work is somewhat different. The calculated midpoint potentials in $\epsilon_s = 37$ at the two probe radii are quite different from each other. With a probe radius of 1.4 Å (rad = 1.4 Å), there is a trend of increasing reduction potentials for the OS1, OS2, and OS3 configurations of the 1^- cluster system, as found in previous calculations. However, with the 3.7 Å probe radius, the predicted positive shift is not found for the OS1, OS2, and OS3 configurations.

The calculated reduction potentials for the 3^- systems are more positive than those calculated previously and are in better agreement with experiment. Particularly good results are obtained with the solvent reaction field represented by $\epsilon_s = 37$. Strictly chemical reversible reduction potentials for 4^- model

(33) Bashford, D.; Gerwert, K. *J. Mol. Biol.* **1992**, *224*, 473−486.
(34) Bashford, D. In *Scientific Computing in Object-oriented Parallel Environments;* Ishikawa, Y., Oldehoeft, R. R., Reynders, J. V. W., Tholburn, M., Eds.; Springer: Berlin, 1997; Vol. 1343, pp 233−240.
(35) Li, J.; Fisher, C. L.; Chen, J.-L.; Bashford, D.; Noodleman, L. *Inorg. Chem.* **1996**, *35*, 4694−4702.

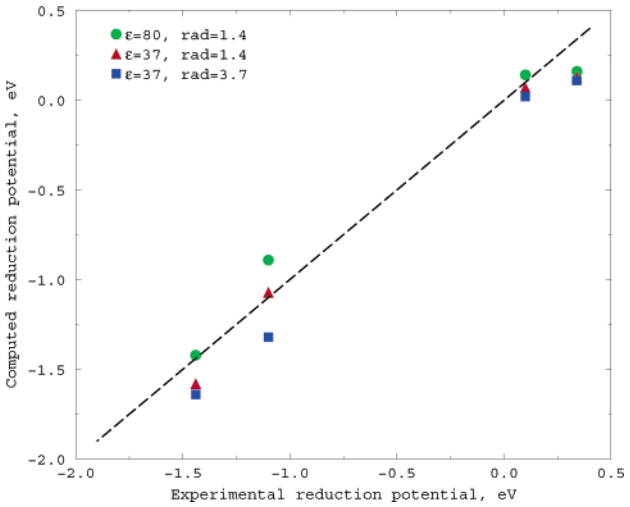

Figure 3. Plot of experimental vs calculated reduction potentials (in eV) for the model $[Fe_4S_4(SCH_3)_4]^{n-}$ (n = 0, 1, 2, 3, 4) systems studied. The dashed line represents the line of identity.

clusters containing thiolate ligands have not been reported, although when given the trend of experimental reduction potential listed in Table 5 and the work of Holm and co-workers, we expect these to be between −1.1 and −2.0 eV.[36]

Experimental geometries associated with the $[Fe_4S_4]^{4+}$ model cluster have not yet been described; thus, no direct comparisons can be made. For the geometry optimizations and subsequent reduction potential calculations, we assume an $S = 0$ broken symmetry state. Here, the ferric centers in the top layer and in the bottom layer are each described by the spin state $|^5/_2\ ^5/_2\ 5>$. When the layers are antiferromagnetically aligned, the resultant $|5\ 5\ 0>$ spin state is generated. The geometrical data for this model cluster at the $S = 0$ spin state is described in Table 1. A pattern of 4:2 long to short distances occurs, although these distances are all relatively short and a result of overlap between the metal-based *d* orbitals in a σ-type interaction. The reduction potential for the all-ferric (0 total charge) model cluster containing alkylthiolate ligands has been estimated to be +0.34 eV.[37] The calculated reduction potential values in Table 5 for the 1−/0 redox couple are in good agreement with this estimate. Here, we have assumed that the OS3 is the final 1− substate for this redox couple; however, there would be little difference if either the OS1 or OS2 substates were used for $\epsilon = 37$, rad = 3.7 Å.

A plot of experimental versus the calculated reduction potentials in this work is shown in Figure 3 and displays the separation of reduction potentials based on redox couple. Of particular interest are the $\epsilon = 37$, rad = 3.7 Å values with which direct comparison to synthetic clusters can be made. It can also be seen that the calculated reduction potentials are generally more negative than the experimental potentials, but the overall correlation with experiment is quite good.

4.2. Reduction Potentials in Proteins. The reduction potentials of iron−sulfur clusters in the protein−solvent environment compared with those of model clusters directly immersed in solvent are quite different. Much effort has focused on understanding the effect of the protein environment on the reduction potential of associated iron−sulfur clusters, with a particular emphasis on elucidating how the protein controls the reduction potential. The principal differences can be typically attributed to general effects or features present only in proteins, including dielectric influence of the medium, electrostatic effects (encompassing hydrogen bonding) of amide dipoles near the active site, and solvent accessibility of the Fe_4S_4 cluster.[12,38−41] In particular, it has been suggested that charge−dipole and dipole−dipole interactions at the active site play key roles in this modulation process.

The protein electrostatic environment that the Fe_4S_4 cluster is exposed to is very different in the HiPIPs, Fd's, photosystem I, and the Fe protein of nitrogenase, and this is likely the main contributor to the observed redox couple in that particular protein. For the proteins studied, it was observed that the number of hydrogen bonds in the active site varied between the types of Fe_4S_4 proteins but generally remained constant within that protein type. For example, there are 5 hydrogen bonding interactions near the active site cluster in the HiPIPs, 10 for the Fd's, and 14 for the Fe protein of nitrogenase. However, deviations from this pattern are seen in the three Fe_4S_4 clusters of photosystem I (*vide infra*).

4.2.1. High Potential Iron Proteins. Two different HiPIP structures were examined: the HiPIP from *Ectothiorhodospira vacuolata* (1hpi, solved at 1.8 Å resolution)[42] and from *Ectothiorhodospira halophilia* (2hip, solved at 2.5 Å resolution).[43] Previous calculations[11,24] on 1− clusters suggested the OS3 state to be the ground state, on the basis of hyperfine properties in the $HiPIP_{ox}$ clusters and proteins. To investigate this, the reduction potentials for all three electronic substates (OS1, OS2, and OS3) in the 1hpi system were determined. The calculated reduction potentials in the protein plus solvent reaction fields are shown in Table 6, which incorporate the amide dipoles within the quantum region ($\epsilon_i = 1$). The reduction potentials obtained here closely approximate the experimentally determined value.[44] For the HiPIP from *E. vacuolata* (1hpi), the reduction potentials using the cluster geometries of the OS1, OS2, and OS3 substates were calculated. The OS3 substate has been proposed to be the redox active form of the $[Fe_4S_4]^{3+}$ cluster in proteins,[11,24,45] on the basis of the analysis of ^{57}Fe hyperfine spectra and Mössbauer isomer shifts.[24,46] We have found that the OS3 substate is slightly more stable than OS1 and OS2 in the protein environment (Table 6); thus, for calculations involving the 2hip protein, from *E. halophilia*,[43] only the OS3 substate geometry and charges were used to calculate the reduction potential. Good agreement between calculated (−0.03 eV) and experimental (+0.120 eV)[47] reduction

(36) Zhou, C.; Raebiger, J. W.; Segal, B. M.; Holm, R. H. *Inorg. Chim. Acta* **2000**, *300*−*302*, 892−902.
(37) Mouesca, J.-M.; Lamotte, B. *Coord. Chem. Rev.* **1998**, *178*−*180*, 1573−1614.
(38) Glaser, T.; Hedman, B.; Hodgson, K. O.; Solomon, E. I. *Acc. Chem. Res.* **2000**, *33*, 859−868.
(39) Backes, G.; Mino, Y.; Loehr, T. M.; Meyer, T. E.; Cusanovich, M. A.; Sweeny, W. V.; Adman, E. T.; Sanders-Loehr, J. *J. Am. Chem. Soc.* **1991**, *113*, 2055−2064.
(40) Eidsness, M. K.; Burden, A. E.; Richie, K. A.; Kurtz, D. M. J.; Scott, R. A.; Smith, E. T.; Ichiye, T.; Beard, B.; Min, T.; Kang, C. *Biochemistry* **1999**, *38*, 14803−14809.
(41) Adman, E. *Proc. Natl. Acad. Sci. U.S.A.* **1975**, *72*, 4854−4858.
(42) Benning, M. M.; Meyer, T. E.; Rayment, I.; Holden, H. M. *Biochemistry* **1994**, *33*, 2476−2483.
(43) Breiter, D. R.; Meyer, T. E.; Tayment, I.; Holden, H. M. *J. Biol. Chem.* **1991**, *266*, 18660−18667.
(44) Heering, H. A.; Bulsink, Y. B. M.; Hagen, W. R.; Meyer, T. E. *Biochemistry* **1995**, *34*, 14675−14686.
(45) Mouesca, J.-M.; Noodleman, L.; Case, D. A. *Int. J. Quantum Chem.* **1995**, *22*, 95−102.
(46) Papaefthymiou, V.; Millar, M. M.; Munck, E. *Inorg. Chem.* **1986**, *25*, 3010−3014.

Table 6. Calculated Reduction Potentials in Fe_4S_4 Proteins (in eV)

protein	total number of amide interactions	$\Delta E_{BS} + \Delta\Delta E_{spin}$[a]	ΔE_{PB}	$E°_{calc}$	$E°_{exp}$
1hpi.pdb (HiPIP, ox)$^{2-/1-}$					
(OS1, $S = {}^1/_2$)	5	−0.17	+4.53	−0.07	+0.170 (ref 44)
(OS2, $S = {}^1/_2$)		−0.10	+4.47	−0.06	
(OS3, $S = {}^1/_2$)		−0.15	+4.48	−0.10	
2hip.pdb (HiPIP, ox)$^{2-/1-}$					
(OS3, $S = {}^1/_2$)	5	−0.15	+4.55	−0.03	+0.120 (ref 47)
1vjw.pdb (Fd)$^{3-/2-}$					
($S = {}^1/_2$)	10	−4.24	+7.97	−0.70	−0.453 (ref 51)
1fxr.pdb (Fd)$^{3-/2-}$					
($S = {}^1/_2$)	10	−4.24	+7.95	−0.72	−0.385 (ref 52)
2fxb.pdb (Fd)$^{3-/2-}$					
($S = {}^1/_2$)	10	−4.24	+8.36	−0.31	−0.280 (ref 53)
1jb0.pdb (PS I)					
($S = {}^1/_2$)$^{3-/2-}$					
X cluster	14	−4.24	+7.69	−0.98	−0.70 (ref 55)
A cluster	12		+8.16	−0.51	−0.55 (ref 55)
B cluster	12		+7.96	−0.71	−0.59 (ref 55)
1g5p.pdb(Fe prot, nitrogenase)					
($S = {}^1/_2$)$^{3-/2-}$	14	−4.24	+8.04	−0.63	−0.310 (ref 25)
($S = 4$)$^{4-/3-}$		−7.33	+10.65	−1.11	−0.800 (ref 56)

[a] The $\Delta\Delta E_{spin}$ values are calculated from the equations given in the Appendix and Table 7.

potentials were found in this system. Examination of the protein environment around the active site cluster reveals that, in both HiPIP proteins, five hydrogen bond (amide−dipole) interactions occurred; one is associated with a bridging sulfur atom, while the remaining interactions were found with the cysteine sulfur ligands.

4.2.2. Ferredoxins. Three different Fd proteins were examined to calculate the reduction potential. The ferredoxin crystal structures used in this calculation were those from *Thermotoga maritima* (1vjw, at resolution of 1.75 Å),[48] *Desulfovibrio africanus* (1fxr, 2.3 Å),[49] and *Bacillus thermoproteolyticus* (2fxb, 2.3 Å).[50] The reduction potentials were calculated for the $S = {}^1/_2$ cluster systems, as this spin state is known to occur experimentally in these proteins, with the results given in Table 6. The calculated reduction potential for the $S = {}^1/_2$ state in *T. maritima* is 0.247 eV more negative than that determined experimentally.[51] Ferredoxin I from *D. africanus* (1fxr) was also examined. The calculated reduction potential for this protein is 0.335 eV more negative than experiment.[52] Reduction potential calculations using the crystal structure of *B. thermoproteolyticus* were also performed, and the results were compared to the published potential of *B. stearothermophilus*[53] (which is the D64E, E81D mutant of *B. thermoproteolyticus*).[50] Reduction potential calculations using the 2fxb crystal structure gave a value state that is in excellent agreement with experiment (0.03 eV more negative). For all the ferredoxins examined, 10 hydrogen bonding interactions were observed in each protein examined: 4 to the bridging sulfur atoms and 6 to the cysteine sulfur ligands.

4.2.3. Photosystem I. Photosystem I is a member of a class of photosynthetic reaction centers that utilize Fe_4S_4 clusters as the terminal electron acceptors. The crystal structure from the thermophilic cyanobacterium *Synechococcus elongatus*, solved at 2.5 Å resolution,[54] was used to calculate the reduction potentials of the three Fe_4S_4 clusters found in this photosystem, known as "X", "A", and "B". Cluster X is located nearest to the membrane which contains the prosthetic groups in photosystem I and is likely the initial recipient of electrons being transferred. The experimental midpoint reduction potentials for the X, A, and B clusters from spinach PS I have been estimated to be −0.70, −0.55, and −0.59 eV, respectively.[55] The lower potential of the X cluster is somewhat unexpected, since there are 12 total hydrogen bonds to both cluster A and cluster B: 5 to the inorganic (bridging) sulfurs and 7 to the ligand sulfurs (more than one interaction per amide group). In contrast, 14 total hydrogen bonds to cluster X were observed in the crystal structure: 6 to the bridging sulfur atoms and 8 to the ligand sulfur atoms. However, the greater solvent access of clusters A and B may contribute to their more positive potentials compared to that of cluster X. Calculated reduction potential values of each cluster, X, A, and B, with just the protein portion of the PS I crystal structure are −0.87, −0.51, and −0.76 eV, respectively. The PS I structure also includes 127 prosthetic groups (3 Fe_4S_4 clusters, 96 chlorophylls, 22 carotenoids, 4 lipids, and 2 phylloquinones) and a Ca^{2+} ion. Reduction potential

(47) Eltis, L. D.; Iwagami, S. G.; Smith, M. *Protein Eng.* **1994**, *7*, 1145−1150.
(48) Macedo-Ribeiro, S.; Darimont, B.; Sterner, R.; Huber, R. *Structure* 1996, *11*, 1291−1301.
(49) Sery, A.; Housset, D.; Serre, L.; Bonicel, J.; Hatchikian, C.; Frey, M.; Roth, M. *Biochemistry* **1994**, *33*, 15408−15417.
(50) Fukuyama, K.; Nagahara, Y.; Tsukihara, T.; Katsube, Y.; Hase, T.; Matsubara, H. *J. Mol. Biol.* **1988**, *199*, 183−193.
(51) Smith, E. T.; Blamrney, J. M.; Zhou, Z. H.; Adams, M. W. W. *Biochemistry* 1995, *34*, 7161−7169.
(52) Hatchikian, E. C.; Cammack, R.; Patil, D. S.; Robinson, A. E.; Richards, A. J. M.; George, S.; Thomson, A. J. *Biochim. Biophys. Acta* **1984**, *784*, 40−47.
(53) Mullinger, R. N.; Cammack, R.; Rao, K. K.; Hall, D. O.; Dickson, D. P.; Johnson, C. E.; Rush, J. D.; Simopoulos, A. *Biochem. J.* **1975**, *151*, 75−83.
(54) Jordan, P.; Fromme, P.; Witt, H. T.; Klukas, O; Saenger, W.; Krauβ, N. *Nature* **2001**, *411*, 909−917.
(55) Chamorovsky, S. K.; Cammack, R. *Photobiochem. Photobiophys.* **1982**, *4*, 195−200.

calculations were also performed including these prosthetic groups (portions of prosthetic groups for which no coordinates were reported were not included). The calculated values became −0.98, −0.51, and −0.71 eV, respectively. Calculation of the reduction potentials of the X and B clusters in the presence of the partial charges associated with the prosthetic groups thus resulted in values that are slightly more negative than experimentally estimated, in agreement with the results seen earlier for iron−sulfur clusters in other environments. It should be noted that the reduction potentials reported in Table 6 incorporate the charges of the iron−sulfur clusters corresponding to the known oxidation states. For example, in the reduction potential calculation of cluster B, the charges used for cluster A correspond to that of the reduced state, while the charges of cluster X correspond to that of the oxidized state. The effects of various combinations of cluster charges on the calculated potentials were also examined (i.e., A_{ox}/B_{ox}, A_{ox}/B_{red}, A_{red}/B_{red}, and A_{red}/B_{ox} charges were tested in the determination of the reduction potential for the X cluster, etc.). The calculated values were found to be insensitive (within 0.02 eV of those presented) to these changes.

4.2.4. Iron Protein of Nitrogenase. The crystal structure of the Fe protein of nitrogenase from *Azotobacter vinelandii* (1g5p),[29] solved at a resolution of 2.2 Å, was used to calculate the midpoint reduction potentials using the $S = {}^1/_2$ spin state of the 3^- model cluster. Calculation of the reduction potential with the $S = 4$ spin state of the 4^- cluster (BS1) including the amide dipole interactions in the active site dielectric region resulted in reduction potentials (Table 6) that are in good agreement with the experimentally determined midpoint potential (−1.11 eV vs −0.800 eV) for the $[Fe_4S_4]^{1+/0}$ redox couple recently measured by Burgess and co-workers,[56] indicating that the reduction potential may be more negative than reported previously (−0.460 eV).[25] The calculated potential for BS2 was found to be 0.28 eV less stable than that of BS1. This is interesting when one considers that the gas-phase energies of BS1 and BS2 are nearly degenerate (Table 2). The charge distribution between BS1 and BS2 are quite different, giving BS1 an enhanced dipole (Table 4), which presumably leads to the greater stability of BS1 in the protein environment. The midpoint potential for the $3^-/2^-$ couple in the Fe protein was also calculated and is 0.320 eV more negative than experiment. A total of 14 hydrogen bonding interactions were found (more than one interaction per amide group to the iron−sulfur cluster was possible): 6 hydrogen bonds to bridging sulfurs could be found, while the remaining interactions were to the cysteine thiolate ligands.

A plot of experimental versus calculated reduction potentials for the various proteins examined in this work is given in Figure 4. As in the plot of experimental versus calculated reduction potential values for model compounds (Figure 3), the midpoint potentials are grouped by redox couple. This plot also displays the aforementioned separation of reduction potentials associated with the different redox couples and the general underestimate of midpoint potentials.

5. Conclusions

The results of these studies show that the geometries and electronic properties of Fe_4S_4 systems are well reproduced in density functional theory using the broken symmetry method. When the geometries of the various oxidation states of Fe_4S_4 are examined, a general expansion of the core is found as the clusters are reduced, in agreement with experiment and previous calculations. The ESP charges indicate that the iron atoms become progressively more positive while the sulfur atoms become progressively more negative across the series (1^-, 2^-, 3^-, 4^-) as the clusters are reduced, in accord with previous calculations on these systems performed in this group. Good agreement between calculated and experimental reduction potentials for model clusters is obtained for the $2^-/1^-$ and $3^-/2^-$ redox couples (within 0.16 eV or 4 kcal/mol). Predicted potentials for the $4^-/3^-$ redox couple also agree qualitatively with available experimental values from analogous clusters. The structural and electronic calculations on the all-ferrous 4^- cluster model in the $S = 4$ spin state show that the calculated distances lie within with the bond distance uncertainties from EXAFS and are also consistent with EPR and Mössbauer data. In addition, the calculated reduction potential for the all-ferric cluster is in good agreement with experimental estimates.

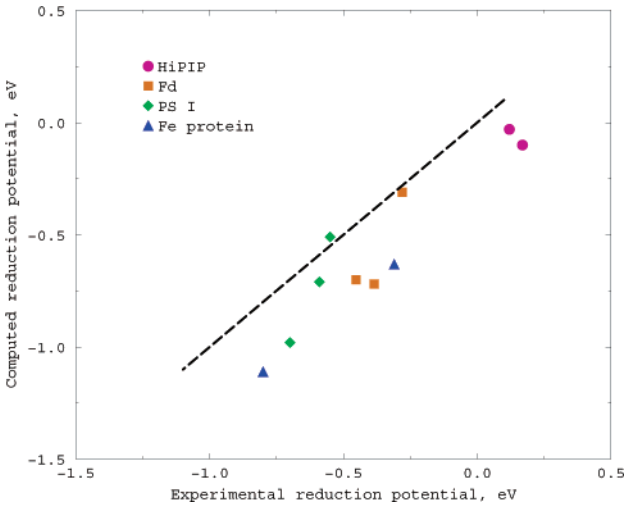

Figure 4. Plot of the experimental vs calculated reduction potentials (in eV) for the protein systems examined, with the dashed line indicating the line of identity.

The fact that our calculated reduction potentials are generally more negative than experiment may be principally due to overestimation of spin-coupling strengths, as indicated by the spin-coupling analysis of Mouesca and Lamotte.[37] Calculated J parameters are typically larger than estimated experimental J parameters.[11,37,45] On the basis of their analysis (see ref 37, Table 7), Mouesca and Lamotte argue that using better experimental J values would lead to positive reduction potential shifts between 0 and 0.3 eV, in good agreement with our observed (experiment to calculated) energy differences.

The observed reduction potentials of the Fe_4S_4 clusters are more negative in solvent than in proteins, and these differences are generally reproduced in the calculations. Overall, the calculated reduction potentials in the protein plus reaction fields displayed a systematic deviation from the experimentally determined potentials, providing estimates that were too negative. In general, agreement with experimentally determined potentials improved when the amide dipoles near the active site were included in the $\epsilon = 1$ dielectric region for the calculations (shown in Table 6 and Figure 4), as discussed in the Computational Methods (section 6). Good agreement between calcu-

(56) Guo, M.; Sulc, F.; Ribbe, M. W.; Farmer, P. J.; Burgess, B. K. *J. Am. Chem. Soc.* **2002**, *124*, 12100−12101.

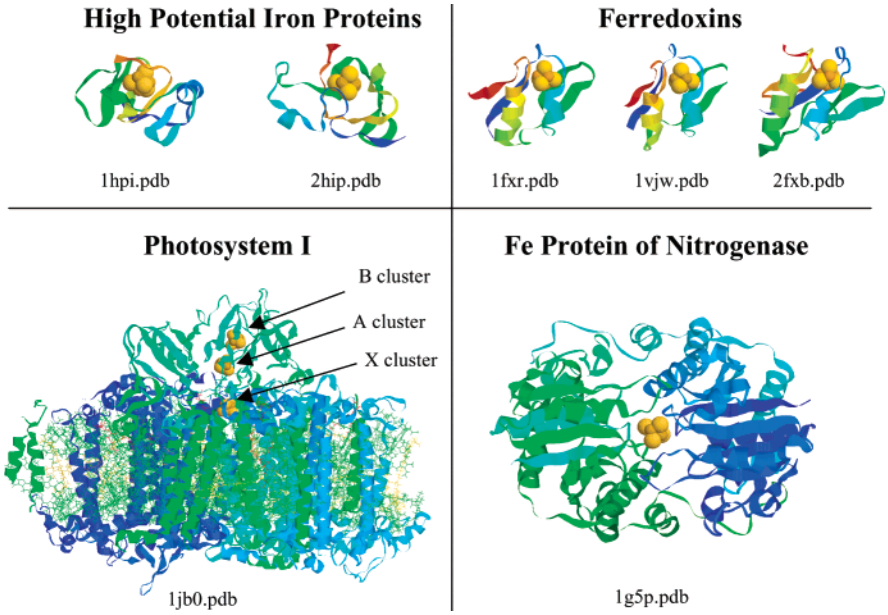

Figure 5. Ribbon drawings of the various proteins on which reduction potential calculations were performed in this study. The figure was made using Rasmol (http://www.umass.edu/microbio/rasmol).

Table 7. Calculated Spin Projection Corrections for $[Fe_4S_4(SCH_3)_4]^{4-,3-,2-,1-}$

system	ΔE_{spin}	J parameter (cm^{-1})	quantitative ΔE_{spin} (eV)
$S = 0$ (0)	$-5J_{ferric}$	907	−0.562
OS 1 (1^-)	$-4J_{OS1}$	725	−0.360
OS2 (1^-)	$-4J_{OS2}$	660	−0.327
OS3 (1^-)	$-[{}^9/_2 J_{OS3} + 5\Delta J_{12(OS3)}]^a$	675	−0.475
$M_S = {}^9/_2$ (1^-)	$-[{}^5/_2 J_{inter} + 5\Delta J_{12}]$	675	−0.259
ref (2^-)	$-{}^9/_2 J_{ref}$	645	−0.360
OC2 (3^-), $S = {}^1/_2$	$-[4J_{red} + B']^b$	519	−0.334
$S = {}^7/_2$ (3^-)	$-{}^5/_2 J_{ref}$	645	−0.20
OC2 (3^-), $S = {}^3/_2$	$-[{}^5/_2 J_{red} + 2B']^b$	519	−0.314
$S = 0$ (4^-)	$-4J_{ferrous}$	112	−0.056
$S = 4$ (4^-)	$-2J_{ferrous}$	112	−0.028
$S = 8$ (4^-)	0	0	−0

[a] $\Delta J_{12(OS3)} = 159\ cm^{-1}$. [b] $B' = 618\ cm^{-1}$. The 2^- cluster is the reference state. [c] Note: All ΔE_{spin} values are stabilization energies for particular states from E_{BS}, that is $(E(S) - E_{BS})$.

lated and experimental reduction potentials in the Fe protein of nitrogenase was obtained, providing reliable cluster geometries corresponding to the electronic properties of the $S = 4$ spin coupled state. The largest deviation among the proteins examined was found in the ferredoxin protein from *D. africanus* (0.335 eV more negative), with errors ranging from 0.03 to 0.34 eV (or 0.7 to 7.7 kcal/mol) too negative. Comparisons among ferredoxins are in somewhat better agreement with experiment than are comparisons between ferredoxins and photosystem I, but there is not enough data to say whether this is a coincidence. A general trend of increasing hydrogen bonding (charge-dipole, dipole−dipole) interactions between the Fe_4S_4 cluster and the protein environment is seen as the cluster becomes more reduced. These interactions likely allow for lower cluster oxidation states to be attained within a physiological range.

A number of previous computational studies have considered what influences reduction potentials and related properties such as reorganization energies in iron−sulfur cubanes. These have generally used quantum chemistry to look at properties of the clusters themselves[37,57] or classical electrostatic models to look at the influence of the protein/solvent environment.[12−14,58−61] Mouesca and Lamotte[37] developed a model, based in large part on earlier DFT calculations,[11] that can be used to estimate reduction potentials for synthetic model clusters. This model builds an estimate of reduction potentials out of three main parts: the intrinsic (or gas-phase) self-repulsion of the negatively charged sulfur atoms with each other; the changes in spin-coupling energies from one redox state to the next (see Appendix); and the solvation energy, as estimated from a simple effective-sphere Born model. This model is quite successful in rationalizing and predicting reduction potentials for a variety of iron−sulfur clusters. Since it is reasonable, empirical, and based on our earlier DFT calculations as well as on experiment, it is not surprising that the results for four-iron cubanes are in good qualitative accord with what we find here. In particular, as in our results, this model predicts an overall range of reduction potentials of about 2 eV when going from the $1^-/0$ to the $4^-/3^-$ redox couple.

Computational studies of the effect of the protein environment have often concentrated (as have experimental studies) on the effects of hydrogen bonds between backbone amides and the sulfur atoms of the cluster.[14,57] More general attempts to estimate all of the relevant features (including solvent accessibility, protein side chains, and so on) have been based on electrostatic models akin to those used here. For example, Banci et al.[13] used a Poisson−Boltzmann dielectric continuum model related to that used here to estimate protein contributions to reduction potentials at the $2^-/1^-$ and $3^-/2^-$ level. Stephens et al.[12] applied a protein dipole/Langevin dipole (PDLD) analysis to 9 iron−sulfur proteins containing 11 four-iron clusters for the same two redox couples. As in Table 6 here, the relative reduction potentials for different proteins were reasonably well reproduced, although

(57) Sigfridsson, E.; Olsson, M. H. M.; Ryde, U. *Inorg. Chem.* **2001**, *40*, 2509−2519.
(58) Capozzi, F.; Ciurli, S.; Luchinat, C. *Struct. Bonding* **1998**, *90*, 127−160.
(59) Jensen, G. M.; Warshel, A.; Stephens, P. J. *Biochemistry* **1994**, *33*, 10911−10924.
(60) Langen, R.; Jensen, G. M.; Jacob, U.; Stephens, P. J.; Warshel, A. *J. Biol. Chem.* **1992**, *267*, 25625−25627.
(61) Smith, E. T.; Tomich, J. M.; Iwamoto, T.; Richards, J. H.; Mao, Y.; Feinberg, B. A. *Biochemistry* **1991**, *30*, 11669−11676.

errors on the order of 0.2 eV between proteins in the same oxidation state were obtained. These methods did not allow any comparisons of reduction potentials between oxidation states and were done before the structures of PS I or an accurate structure of the iron protein of nitrogenase were known. For further analysis of these earlier calculations, see Li et al.[19] The current calculations represent the first attempts to estimate absolute reduction potentials in Fe_4S_4 proteins in a way that includes (at least in an approximate fashion) all the physically important interactions. In particular, the large reorganization free energies that, in this model, arise from dielectric relaxation include both enthalpic and entropic contributions. Additional improvements in the calculated reduction potentials may be possible by expanding the quantum mechanically treated region to include factors such as charge transfer (associated with hydrogen bonding interactions with the cluster), better treatment of prosthetic groups in protein environment, relaxation of the protein from its crystal environment, vibrational zero point and entropy effects, and further changes in the protein structure that occur upon reduction. These are topics of future work, but reasonably good estimates of reduction potentials for the Fe_4S_4 clusters may be obtained using the procedure outlined here.

6. Computational Methods

The Amsterdam Density functional (ADF, version 2.3) [62−64] package was used to calculate the geometries and associated gas-phase energies of the iron−sulfur clusters in this study. The spin-unrestricted calculations were performed with an accuracy parameter of 4.0. Basis set IV was used to describe all atoms and consists of uncontracted triple-ζ Slater-type orbitals (STO) for the 4s and 3d valence orbitals, with a single 4p polarization and 3s, 3p inner orbitals for Fe; 3s and 3p orbitals for S, augmented with a 3d polarization function; 2s and 2p valence orbitals of C, N, O that have been augmented with a 3d polarization function; and a triple-ζ STO for the 1s of H with a 2p polarization function.[65,66] The inner core shells were treated by the frozen core approximation up to and including Fe(2p), S(2p), and C(1s) with the core orbitals orthogonal to the valence orbitals. The local density approximation (LDA) utilized the parametrization of Vosko, Wilk, and Nusair (VWN), while the nonlocal corrections for exchange (Becke)[67] and correlation (Perdew)[68,69] were included in each self-consistent field cycle.

The starting structure was based on an idealized experimental geometry consisting of an average iron−iron (Fe−Fe) distance of 2.76 Å, average iron−inorganic sulfur (Fe−S*) distances of 2.25 Å, and average iron−thiolate sulfur (Fe−S) distances of 2.31 Å.[70−72] From this general framework, a single point, high spin calculation was performed at each total cluster charge to obtain the high spin wave function. The electron spin density is then polarized in opposite directions for each subunit, and the subunits are allowed to interact, as described by the broken symmetry method.[73] In this approach, a distinction is made between the geometrical and electronic point symmetry of a molecule. First, the molecule of interest at a particular geometry is considered to be composed of two subunits, thus each Fe−Fe layer can be considered as distinct. The high spin (ferromagnetically coupled) state of the molecule is constructed where the spins on each subunit are aligned in a parallel fashion. For the broken symmetry (antiferromagnetically coupled) state, the spins are arranged in a spin-coupling pattern to achieve the correct net spin. This consideration results in a lowering of the electronic symmetry while retaining the geometric symmetry, and the broken symmetry calculation is performed at the lower point symmetry. SCF convergence was achieved when the change in the mean of the diagonal elements of the density matrix was less than 3×10^{-5} and 1×10^{-3} in the norm of all gradients. The accuracy parameter for the numerical integration[63] grid was 4.0. Spin populations were determined by a Mulliken analysis. Discussion of metal-based d-orbital overlap in the all-ferrous model clusters refers to overlap of parallel-aligned minority spin−orbitals and utilizes the same coordinate axis as given in Figure 2.

Molecular electrostatic potentials (MEPs) were then generated from the fit that was least-squares fit to a set of point charges (electrostatic potential, ESP, charges) centered on the atoms. The ESP charges for each cluster were calculated using a modified version of the CHELPG code of Breneman and Wiberg[74] and the ADF codes using Chargefit, where the total net charge of each cluster and the dipole moment were utilized as constraint conditions for the charge fitting. The van der Waals radii used for the atoms for the charge fitting procedure were as follows: Fe(2+/3+), 1.3 Å; S, 1.8 Å; C, 1.7 Å; H, 1.2 Å. Symmetry equivalent atoms gave rise to ESP charges that were equivalent. The singular value decomposition (SVD) method[75] was incorporated to minimize the uncertainties in the fitting procedure and provide a model with stable atomic charges corresponding to the molecular dipole moment.[11,19,22,35] The set of point charges generated represents the best fit of the MEP calculated by nonlocal DFT methods.

The ESP charges were utilized in the MEAD (Macroscopic Electrostatics with Atomic Detail) program suite[33,34] to calculate the reaction field energies using the macroscopic Poisson or Poisson−Boltzmann equation. In MEAD, the solute is represented by a set of atomic charges and van der Waals (vdW) radii, while the solvent is represented as a continuous dielectric medium. In the case of the model cluster system, the reaction field was generated by solvent polarization: each cluster was immersed in a continuous dielectric representing the solvent ($\epsilon_s = 37, 80$) and only the solvent is allowed to polarize, in response to the cluster charge distribution. The atomic radii for the cluster atoms were identical to those used for the charge fitting procedure. The solvent inaccessible volume of the solute in $\epsilon_s = 37$ used the Connolly[76] radius (1.4 Å) and a radius of 3.7 Å, to approximate the radius for solvents such as acetonitrile and *N*,*N*-dimethylformamide (DMF; Han & Noodleman, unpublished results). This radius was calculated by adding the maximum atomic distance of the atoms within the solvent molecules and the vdW radii of these atoms and then dividing the total by two. For calculation of the protein field and reaction field energies in the protein, the PARSE charge and radii set was used to determine the charge distribution for the protein atoms,[77] and a solvent inaccessible volume of the solute[76] was used to represent the boundary between the solute and the solvent (for $\epsilon_s = 80$). In the case of the Fe_4S_4 clusters in the protein, the reaction field was generated by polarization from the protein plus the surrounding solvent in response to the cluster charge distribution. The protein field was generated by the protein charges which are screened by the dielectric media and act on the cluster charges. The "dual boundary" approach was utilized to ensure charge conservation with regard to the active site cluster and to avoid nonphysical charge interactions between H atoms of the model cluster and the Cα atoms in the protein.[19] The protein plus solvent

(62) *ADF*, 2.3.0 ed.; Free University of Amsterdam: The Netherlands, 1997.
(63) te Velde, G.; Baerends, E. J. *J. Comput. Phys.* **1992**, *99*, 84−98.
(64) Baerends, E. J.; Ellis, D. E.; P., R. *Chem. Phys.* **1973**, *2*, 41−59.
(65) Snijders, J. G.; Baerends, E. J.; Vernooijs, P. *Atomic Nuclear Data Tables* **1982**, *26*, 483.
(66) Vernooijs, P.; Snijders,: J. G.; Baerehds, E. J. *Slater Type Basis Functions for the Whole Periodic System*; Free University of Amsterdam: The Netherlands, 1981.
(67) Becke, A. D. *Phys. Rev. A* **1988**, *38*, 3098−3100.
(68) Perdew, J. P. *Phys. Rev. B* **1986**, *33*, 8822−8824.
(69) Perdew, J. P. *Phys. Rev. B* **1986**, *34*, 7406.
(70) Averill, B. A.; Herskovitz, T.; Holm, R. H.; Ibers, J. A. *J. Am. Chem. Soc.* **1973**, *95*, 3523−3534.
(71) Berg, J. M.; Hodgson, K. O.; Holm, R. H. *J. Am. Chem. Soc.* **1979**, *101*, 4586−4593.
(72) O'Sullivan, T.; Millar, M. M. *J. Am. Chem. Soc.* **1985**, *107*, 4096−4097.
(73) Noodleman, L.; Baerends, E. J. *J. Am. Chem. Soc.* **1984**, *106*, 2316−2327.
(74) Breneman, C. M.; Wiberg, K. B. *J. Comput. Chem.* **1990**, *11*, 361−373.
(75) Francl, M. M.; Carey, C.; Chirlian, L. E.; Gange, D. M. *J. Comput. Chem.* **1996**, *17*, 367−383.
(76) Connolly, M. L. *Science* **1983**, *221*, 709−713.
(77) Sitkoff, D.; Sharp, K. A.; Honig, B. *J. Phys. Chem.* **1994**, *98*, 1978−1988.

reaction field is divided into three dielectric constant regions: $\epsilon_i = 1$ for the active site (cluster), $\epsilon_p = 4$ for the protein, and $\epsilon_s = 80$ for the solvent. Here, the Poisson equation is solved at zero ionic strength. The standard reduction potential, $E°$, is calculated by adding the gas-phase ionization potential for the reduced species, IP(red), to the solvation energy difference (ΔE_{PB}) of the oxidized minus the reduced state, including the spin projection correction (ΔE_{spin}, see Appendix for details), and referencing the resulting value to the standard hydrogen electrode (ΔSHE, −4.43 eV),[78] as shown in eq 1.[11]

$$E^0 = IP(red) + \Delta E_{PB} + \Delta\Delta E_{spin} + \Delta SHE \quad (1)$$

Calculations of the midpoint potentials in the protein environment were conducted on two high potential iron proteins (Protein data bank[79] reference codes: 1hpi and 2hip), three ferredoxin proteins (1vjw, 1fxr, and 2fxb), photosystem I (1jb0), and the iron protein of nitrogenase (1g5p). In each case, the positions of the iron and bridging sulfur atoms from the optimized clusters were least-squares fit to the corresponding atoms in the active site of the X-ray structure; the remaining atomic positions were taken from the published X-ray coordinates. In this way, the effect of the different ligand conformations on the reduction potential for each protein was taken into account. The reduction potential for each protein was calculated, including backbone amide interactions near the active site. This was accomplished by including the O═C···NH atoms in the active site dielectric region ($\epsilon_i = 1$), rather than in the protein dielectric region ($\epsilon_p = 4$). The physical idea underlying this model is that hydrogen bonds to the cluster tend to inhibit protein mobility at this interface, so there is little protein dielectric screening and $\epsilon_s = 1$ is an appropriate dielectric constant over the region of the hydrogen bonded amides. The number of amide dipoles near the active site varied between the types of Fe_4S_4 proteins but remained constant within that protein type. For example, there are 5 amide dipoles near the active site cluster in the HiPIPs, 10 for the ferredoxins, 7−9 for the three clusters in PS I, and 10 for the Fe protein of nitrogenase. For a more detailed explanation of these methods, we refer the reader to previous work on these systems.[11,19] Charges for the prosthetic groups (except the iron−sulfur clusters) were derived using the Antechamber module of AMBER.[80] For the chlorophylls in PS I, charges were generated separately for the Mg^{2+}-corrin ring and for the hydrophobic tail. In instances where atoms were not present in the crystal structure for a respective prosthetic group, charges were redistributed within that group to maintain an integer charge.

Acknowledgment. This work was supported by NIH Grant GM39914. We thank Wen-Ge Han for helpful discussions, E. J. Baerends and the Theoretical Chemistry Group at the Free University of Amsterdam for the ADF codes, and Donald Bashford for use of the MEAD codes.

9. Appendix

Spin-Coupling Corrections. We present a summary for relating the energies of the broken symmetry states E_{BS} to the corresponding lowest energy pure spin states $E(S)$. The spin Hamiltonian correction is $H = J(S_1 \cdot S_2)$ This allows one to determine corrections to the broken symmetry energy differences due to spin projection for the reduction potentials. Table 7 presents the spin projection stabilization energies, $\Delta E_{spin} = E(S) - E_{BS}$, for a variety of clusters and redox states, both quantitatively and as equations. These energy differences are derived by referencing both $E(S)$ and E_{BS} to the high spin state energy $E(HS) = E(S_{max})$.

Most of the iron sites in Fe_4S_4 clusters occur in equivalent pairs.[83] We examine these first and then consider the rarer, nonpairwise equivalence patterns. The cubanes are referred to by total cluster charge (0, 1^-, 2^-, 3^-, 4^-). From the starting point of all ferric (0) and $HiPIP_{ox}$ (1^-), the clusters have zero, one, two, one, and zero mixed valence ($Fe^{2.5+}-Fe^{2.5+}$) delocalized pairs, respectively. For (1^-), the alternate Fe pair is ($Fe^{3+}-Fe^{3+}$), while, for the (3^-), the alternate pair is ($Fe^{2+}-Fe^{2+}$). The (4^-) cluster is all ferrous (4 Fe^{2+}) and contains no mixed valence pairs. All systems with one or two mixed valence pairs have a spin Hamiltonian parameter B related to resonance delocalization within a mixed valence pair. There is also, in the case of the 3^- cluster, an interpair delocalization parameter B' for the resonance between the mixed valence and ferrous pairs of reduced ferredoxin. However, the main pairwise mixed valence delocalization energy is the same for the broken symmetry and the corresponding pure spin state energies and, therefore, does not appear in the ΔE_{spin} equations.

For the all-ferric cluster, each diferric layer has spins $S_{dimer} = 5$. The high spin ($S_{tot,max} = 10$) minus the broken symmetry energy is

$$E(S_{tot,max} = 10) - E(BS) = J[(S^2_{tot,max}/2)]$$

while the E(HS) minus singlet ($S = 0$) energy difference is

$$E(S_{tot,max} = 10) - E(S = 0) = J[(S_{tot,max}(S_{tot,max} + 1))/2]$$

The difference between these equations gives the $\Delta E_{spin} = E(S = 0) - E(BS)$ values reported in Table 7.

Using eq 5 and Table 2 from Mouesca et al.[11] provides the corrections for the OS1 and OS2 substates of the 1^- cluster, for the 2^- cluster, and for the 3^- cluster. For the OS3 substate of the 1^-cluster, we use the more accurate results based on a six parameter fit to the BS and HS state energies,[45] instead of the earlier three parameter fit.[11] Of the six parameters, only two appear in ΔE_{spin}. We define J as the interlayer Heisenberg coupling parameter between a mixed valence $Fe^{2.5+}$ and an Fe^{3+} site for the electronic substates OS1, OS2, and OS3. The parameter $\Delta J_{12} = J(Fe^{3+}-Fe^{3+}) - J(Fe^{2.5+}-Fe^{3+})$ represents the difference between the diferric pair J parameter and the interlayer J parameter.

The other ΔE_{spin} results in Table 7, like those earlier, require straightforward spin algebra based on the following equation for HS versus BS alignment of two coupled site spins, A and B:

$$\langle \vec{S}_A \cdot \vec{S}_B \rangle_{HS} = +S_A S_B \quad (A1)$$

$$\langle \vec{S}_A \cdot \vec{S}_B \rangle_{BS} = -S_A S_B \quad (A2)$$

as shown in Mouesca et al., 1994[11] (see eq 5 and Discussion). The energies are then compared with the closely related pure spin state $E(S)$, where S = total spin, referenced to the high spin state energy.

(78) Reiss, H.; Heller, A. *J. Phys. Chem.* **1985**, *89*, 4207−4213.
(79) http://www.rcsb.org/pdb.
(80) Case, D. A.; Pearlman, D. A.; Caldwell, J. W.; Cheatham, T. E. I.; Wang, J.; Ross, W. S.; Simmerling, C. L.; Darden, T. A.; Merz, K. M. J.; Stanton, R. V.; Cheng, A. L.; Vincent, J. J.; Crowley, M. F.; Tsui, V.; Gohlke, H.; Radmer, R. J.; Duan, Y.; Pitera, J.; Massova, I.; Seibel, G. L.; Singh, U. C.; Weiner, P. K.; Kollman, P. A.; *AMBER*, 7th ed.; University of California: San Francisco, CA, 2000.
(81) Flukiger, P.; Luthi, H. P.; Portmann, S.; Weber, J.; *MOLEKEL*, version 4.1; Swiss Center for Scientific Computing: Manno, Switzerland, 2000.
(82) Mascharak, P. K.; Hagen, K. S.; Spence, J. T.; Holm, R. H. *Inorg. Chim. Acta* **1983**, *80*, 157−170.
(83) Beinert, H.; Holm, R. H.; Munck, E. *Science* **1997**, *277*, 653−659.

The $HiPIP_{ox}$ OS3 substate (broken symmetry) has the spin of the ferric pair ($S_{12} = S(Fe^{3+}-Fe^{3+})$) parallel aligned to give $S_{12} = 5$. For the $M_S = {}^9/_2$ broken symmetry state, these spins are oppositely aligned (see Figure 1a; $S = {}^9/_2$, bottom layer), and the closest pure spin state has $S_{12} = 0$, $S_{34} = {}^9/_2$, and total $S = {}^9/_2$. The pure spin ground state in this system is expected to be somewhat canted, so that $S_{12} = 4$, $S_{34} = {}^9/_2$, and total $S = {}^1/_2$ because of the stronger J coupling in the $Fe^{3+}-Fe^{3+}$ pair than the other J couplings.[24] This is taken into account for the entries in Table 7 for OS3 and $M_S = {}^9/_2$ (1^-). The J parameters for OS3 and $M_S = {}^9/_2$ are common to both, $J_{OS3} = J_{inter}$ and $\Delta J_{12} = \Delta J_{12(OS3)}$, and $J(Fe^{3+}-Fe^{3+}) = J_{OS3} + \Delta J_{12(OS3)}$. As seen from this argument, the spin state $S = {}^9/_2$ is at a considerably higher energy than the ground state $S_{12} = 4$, $S_{34} = {}^9/_2$, $S = {}^1/_2$ by 0.86 eV.

Next, we consider the OS1 and OS2 electronic states of $HiPIP_{ox}$-type clusters compared with OS3. These have calculated energies that are very close to that of OS3 (spin canted) when synthetic clusters or protein environments are considered (see Tables 5 and 6, next to last column). Strictly on lowest energy alone, one would expect that OS1 would be the lowest energy state from the calculation in dielectric medium ($\epsilon = 37$), and OS3, in the protein environment, since the most negative reduction potential corresponds to the most stable oxidized state of the $2^-/1^-$ couple. The OS1 and OS2 electronic configurations are generated by starting from the OS3 BS state ($S_{12} = 5$) and performing a single spin forbidden transition on the diferric pair for each to generate $S_{12} = 4$. These transitions are a combination of spin forbidden charge-transfer CysS $\rightarrow$ Fe and spin forbidden Fe d $\rightarrow$ d so that a combination of $S_1 = {}^3/_2$, $S_2 = {}^5/_2$ or $S_1 = {}^5/_2$, $S_2 = {}^3/_2$ in resonance produce $S_{12} = 4$. Here, the site spins may involve some radical character on the cysteine sulfur, which is also true for OS3. In contrast to the OS3 pure spin ground state, OS1 and OS2 are not spin canted states, and the BS forms have the same pair spin combination $S_{12} = 4$, $S_{34} = {}^9/_2$ as the corresponding lowest pure spin states.

For the reduced ferredoxin (3^-) type cluster, we find a valence trapped $S = {}^7/_2$ which is nearly degenerate with, but slightly above (by 0.06 eV, Table 5), the calculated $S = {}^1/_2$ ground state for the cluster in a dielectric medium of $\epsilon = 37$. The trapped Fe^{3+} site spin is flipped with respect to the three Fe^{2+} sites (Figure 1c). We also note the very near degeneracy between $S = {}^1/_2$ and $S = {}^3/_2$, both based on the same broken symmetry OC2 state (Table 7). Experimentally, it is well-known that $S = {}^1/_2$ and $S = {}^3/_2$ can be nearly degenerate in both synthetic systems and in proteins (i.e., in the reduced (3^-) nitrogenase Fe protein). In selenium substituted *Clostridium pasteuranum* ferredoxin (3^-), $S = {}^1/_2$, ${}^3/_2$, and ${}^7/_2$ are known to be nearly degenerate at very low (1.6 K) temperatures (see Noodleman, 1991[84] and references therein).

Finally, for the all-ferrous (4^-) complex, we performed a single J parameter fit to the broken symmetry energy differences with respect to the high spin $S = 8$ state for both BS1 and BS2 ($M_S = 4,0$), giving the corresponding pure spin states $S = 4$ and $S = 0$. The one parameter J fit has an RMS error of ± 0.045 eV for the total energy difference $28J = E(HS) - [(E(BS1) + E(BS2))/2]$, which is very acceptable in view of the size of other energy terms in the calculations and their uncertainties (J parameter uncertainty $= \pm 13$ cm^{-1}). The ΔE_{spin} stabilization energies for the all-ferrous $S = 4$ and $S = 0$ are small compared to those of all the other oxidation states. Mainly, the spin stabilization energies are larger when J is larger (more antiferromagnetic). The spin canting is a significant contributor to the enhanced ΔE_{spin} in OS3(1^-). Further, one should recall that the broken symmetry states themselves contain the main antiferromagnetic Heisenberg coupling and the main resonance delocalization energies.

JA0211104

(84) Noodleman, L. *Inorg. Chem.* **1991**, *30*, 246−256.